Anadolu Üniversitesi Bilim ve Teknoloji Dergisi A- Uygulamalı Bilimler ve Mühendislik
Anadolu University Journal of Science and Technology A- Applied Sciences and Engineering

ANADOLU UNIVERSITY

2017 - Volume: 18 Number: 2
Page: 388 - 397
DOI: 10.18038/aubtda.295720
Received:01 March 2017 Revised: 18 April 2017 Accepted: 28 April 2017

OPTICAL VIBRATIONAL AND MORPHOLOGICAL PROPERTIES OF S-Co_3O_4 NANOSTRUCTURED THIN FILM

Tülay HURMA*

Department of Physics, Faculty of Science, Anadolu University, TR-26470, Eskişehir, Turkey

ABSTRACT

Sulphur doped Co_3O_4 (S-Co_3O_4) nanostructured thin film has been deposited on glass substrate. The film has been characterized by X-ray diffraction (XRD), energy-dispersive X-ray spectroscopy (EDS), Fourier transform infrared (FTIR) and Raman spectroscopy. The surface appearance of the film was obtained using scanning electron microscopy (SEM) and atomic force microscopy (AFM). A double beam spectrophotometer equipped with an integrating sphere was used to measure the transmittance and reflectance measurements. Refractive index, extinction coefficient, optical conductivity and dielectric constant of the film were calculated. The XRD pattern shows that the film has only clear diffraction peak around $2\theta = 29.26^o$ corresponding to the (111) plane of cubic Co_3O_4. The crystallite size was calculated to be approximately 24 nm. The Raman measurement revealed four peaks of Co_3O_4. FTIR spectrum of the film has been investigated in 500-3000 cm^{-1} region.

Keywords: S doped Co3O4; XRD; Optical constant; FT-IR; Raman

1. INTRODUCTION

Rapid development of studies conducted on nanotechnology has increased importance of nanoparticles used in several fields. The main reason attracting interest on these materials is that physical and chemical characteristics of these materials undergo a change compared to known rules of physics as the particle subsides into nanosize and surface area increases. At this scale, currently the principles of quantum physics become prevailing rather than the principles of Newton physics. The purpose of analyzing structures with particles smaller than 100 nm is to assay their physical and chemical characteristics and develop production processes for products with superior characteristics. Nanotechnology process has begun with these studies and there have been developments in several fields such as electronics, magnetic, optics and etc. [1, 2]. Due to improvements in production methods and acquired knowledge, the metal, metal-oxide and nanoparticles with various characteristics can be improved by combining. Transition metal oxides are the materials with significant role in several disciplines of material science due to their superior characteristics and wide fields of use [3-6]. Especially, cobalt-oxide is one of the most used ones of transition metal oxides. Cobalt-oxide based materials draw great interest due to their potential practices in scientific and technological fields. Cobalt-oxide especially gets attention as a promising material in the energy and environment related practices. Particularly, successful results have been obtained in artificial photosynthesis systems by using cobalt-oxide nanoparticles [7-9]. Cobalt-oxide is usually present in three different cystalline forms as CoO, Co_2O_3 and Co_3O_4. Thanks to its various chemical stability and intended electrochemical properties, all stoichiometry, Co_3O_4 is used for various application fields [10]. P-type transition metal oxide materials with Co_3O_4 nanostructure (direct band gaps at 1.48 and 2.19 eV) [11] have wide range of usage fields such as solid-state sensors, absorbers of solar energy [12], solar cells and photodetectors [13]. Cobalt oxide and cobalt sulfide materials are synthesized by various methods such as chemical bath deposition [14-16], chemical vapour deposition [17-18], electrochemical deposition [19, 20] and spray pyrolysis technique [10, 21]. In recent years, performance values of metal oxides have been tried to be increased by introducing various dopants [22]. Stella et al. has reported that Fe doped on his C o_3O_4 has caused contraction for particle size compared

*Corresponding Author: tulayhurma@gmail.com

with undoped and Mn doped films, Mn and Fe implantations have resulted in expansion of absorption in the visible section and there has been a shift in the forbidden energy range [23]. Kerli has reported that Bo doped on his Co_3O_4 film which he produced by spray method has distorted the crystal form, changed the forbidden energy range and increased the optical transmittance values [24]. Chtouki et al. has reported that when Zn is included in the Co_3O_4 film, it changes preferred orientation and increases surface smoothness [25]. The main purpose of this study is to report the structural, optical, morphological and vibrational (FT-IR and Raman) characteristics of S doped Co_3O_4 thin film with nanostructure obtained by ultrasonic spray pyrolysis (USP) method.

2. EXPERIMENTAL PROCEDURE

S-Co_3O_4 nanostructured thin film is deposited by using USP method which draws attention by its cost-efficiency and easy application. S-Co_3O_4 thin film was prepared using 0.05M equimolar solutions of $CoCl_2$ and 0.05M equimolar solutions of $(NH_2)_2CS$. To produce the nanostructured film, USP technique was used following the process reported in our previous study [26]. S-Co_3O_4 film has been formed on glass substrate at 300 ±5°C substrate temperature. Substrate temperature has been provided through an electric heater and the temperature has been controlled by using Fluke 62 max infrared thermometer. Nitrogen gas at 0.2 kg/cm^2 pressure has been used as the carrier gas. Spray time has taken almost 20 minutes and 75 ml solution has been sprayed in total for the film. Film thickness has been measured by using an Ellips SC620 Spectroscopic Ellipsometer. Film thickness has been approximately determined as 215 nm. XRD diffraction pattern measurement to determine the crystall forms and phases of obtained thin film has been resulted in between the range of 20°–70° by using Phillips X-ray diffractometer device by using CuK_α beam at $\lambda_{K\alpha}$=1.5406 Å wavelength. SHIMADZU UV 2450 spectrometer has been used for optical absorption and reflectance measurements. Surface characteristics have been analyzed by means of the surface photographs taken by ZEISS EVO-50 model SEM microscope. Average crystalline size has been determined by conducting XRD analysis. FTIR measurement has been conducted in room temperature at 500-3000 cm^{-1} range by means of ATR (4 cm^{-1} resolution) and using Perkin Elmer 2000 FT-IR spectrometer. Raman spectroscopy as well as X-ray diffraction spectroscopy have been used for determining the phase compositions of the film. Raman measurement has been conducted at 100-1000 cm^{-1} range by Bruker Senterra Dispersive Raman system and using laser excitation with 532 nm wavelength.

3. RESULTS AND DISCUSSIONS

3.1. X-ray Diffraction Pattern of the Film

In this study, structural characterization of the film has been analyzed by means of XRD. XRD method is based on the fact that each crystal based on specific atomic packing of phases refracts the X-rays in a characteristic order. K-series beams are especially used in X-ray diffractions. These diffraction profiles of each crystal for the phase defines the related crystal like a fingerprint. Phases in them material and concentration of these phases provide information on the amount and crystal size of noncrystalline phases. XRD diffraction patterns of a 215 nm thick S-Co_3O_4 film have been evaluated for the 20^o to 70^o range. Figure 1 shows the EDS spectrum and XRD pattern of the S-Co_3O_4 film. The diffraction peak seen at 2θ=29.26^o corresponds to the cubic [JCPDS card no 9-418] reflections of Co_3O_4 at (111) plane. Although XRD peak related with its plane is usually observed around 2θ=28,10^o for undoped Co_3O_4 (111), peak observed for [7] S-Co_3O_4 (111) plane was observed at 2θ=29.26^o. This shift showed that sulphur went into Co_3O_4 lattice and the doping process was successful. The cause of shifts of peaks to lower or higher values is enlarging or shrinking of the crystal lattice, in other words translocation of doping atoms with existing atoms by penetrating into the crystal structure [27, 28]. Another diffraction peak is at 2θ=36.30° corresponding to the (210) plane of CoS_2 (JCPDS card no 00-041-1471) and it is also seen at comparatively lower intensities. No other important peak corresponding to other phases of cobalt oxide and cobalt sulphur have not been observed. XRD pattern shows abroad hump-like feature

in the range of 20°-40° which can be attributed to the amorphous nature of glass substrate. The film contains two phases as Co_3O_4 and Co_2S. Crystallites are coherent diffraction domains in X-ray diffraction. Crystalline size can be calculated by using Scherrer equation. According to Scherrer formula, crystalline size can be found based on the following equation with the peak corresponding to the (111) plane (2θ = 29.26˚) [29];

$$D = \frac{K\lambda}{\beta \cos\theta} \tag{1}$$

Here, K indicates a constant, λ indicates the wavelength of the used X-ray, θ indicates Bragg reflection angle and β indicates the full width at half maximum (FWHM). For calculations, K constant is fixed as 0.9. The crystallite size of the film has been determined to be 24 nm.

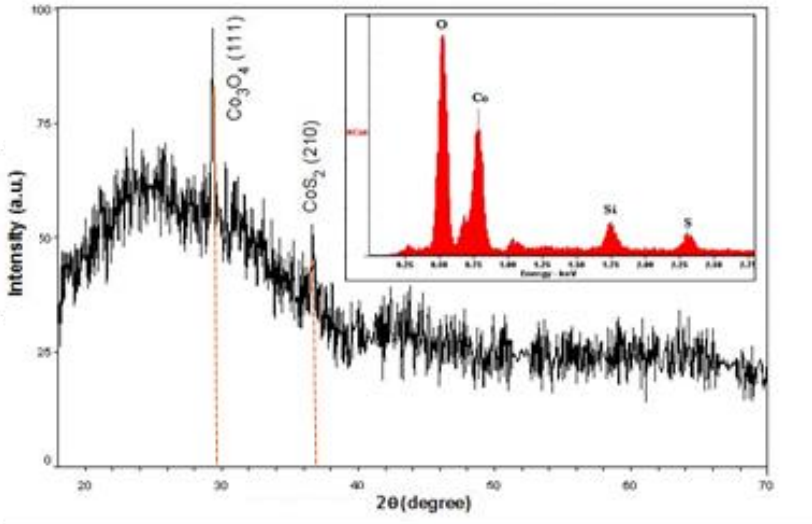

Figure 1. XRD pattern of S-Co_3O_4 nanostructured thin film inset shows the EDAX spectrum

3.2. SEM and AFM Images of the Film

Images from SEM and AFM microscopes help us determining the morphology and particle size of semiconductor films on glass substrate. Figure 2 and 3 show SEM and AFM images of S-Co_3O_4 nanostructured film respectively. The nanosize of particles of the film was estimated from the SEM and AFM images. The SEM image shown in Figure 2 is showing some agglomerated-like structure nearly 100 nm in size. An idea about the particle size is obtained from the SEM photograph and it helps to arrive on the range of particle size. The actual particle size can be larger than "XRD crystallite size" calculated from Scherrer equation. It has been observed from SEM photographs taken with x100.000 magnification that the surface is flat and like a surface covered by fine plant leaves and nanoparticles come together and created such an image. There are observable spaces on the film surface seen as covered by fine plant leaves and it has been determined that the film is formed on the glass base successfully. Figure 3 shows the changes on elevations of the three-dimensional surface structure of the film which is obtained by scanning 5µm x 5µm space of the film by means of AFM. It is seen that the highest surface roughness is around 100 nm. The white regions seen on the surface indicate the clusters due to conglomeration of atoms; the dark regions indicate the gaps on the surface. The gaps were seen dark as the atoms sprayed to surface while forming the film did not prefer these locations. Sulphur doping contributed in uneven surface of the Co_3O_4 film. Porous nanostructure is highly desired to ameliorate the electrochemical properties of catalysts such as Co_3O_4 [10, 30, 31].

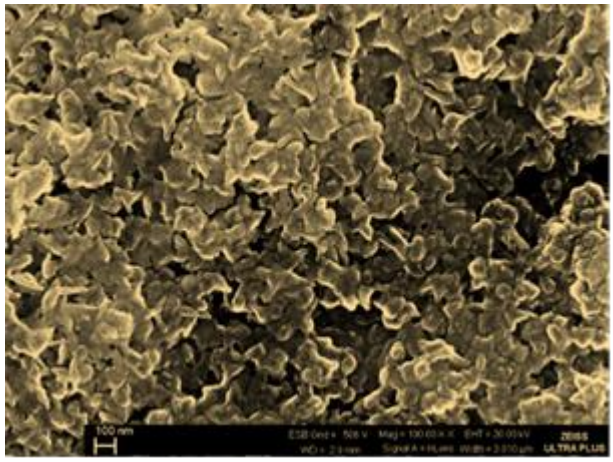

Figure 2. SEM image of the nanostructured thin film under the magnification ×100 000

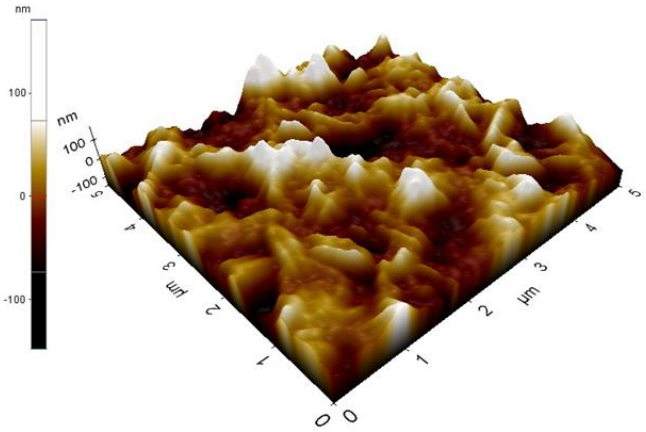

Figure 3. AFM image of the nanostructured thin film

3.3. Optical Properties of the Film

If, the beam reflected matter is a semiconductor, photons react with this material and several optical events such as absorption, diffraction, reflection, penetration and etc. happen. Optical transmittance and reflection spectra were obtained to reveal the optical properties of the S-Co_3O_4 nanostructured thin film. The transmittance and reflectance spectra of the S-Co_3O_4 film are shown in Figure 4. The average value of optical transmission for the nanostructured thin film in the visible range (400-800 nm) was found to be 50%. Transmittance first increases and in wavelength the value reaches to a maximum and then slowly decreases, and again increases and reaches its maximum value. Reflectance first increases relatively sharply with wavelength then slowly increases and reaches its maximum value near the absorption edge. Reflectance value observed for S-Co_3O_4 film is smaller than the reflectance value determined for undoped Co_3O_4 in the literature [32]. It can be seen that film has two step transition. In the study, similar results were reported for the undoped Co_3O_4 film. [7, 10, 33, 34]. Further more, similar results were observed for B doped [35] and Fe doped [36] Co_3O_4 films. According to the study of Wang S. et al. [33] optical absorption and accordingly transmission property are deeply relative to the valence state of the cobalt oxide. Reflection capacity and permeability of thin films are based on factors such as film thickness, refractive index and extinction coefficient. Diffraction as one of the interactions of beams

with materials is the direction change of beams while beams do not reflect vertically on the material or in general sense while they change medium. The values of refractive index are the indicators whether the surface is a reflective or an absorber one. Refractive index (n) of S-Co_3O_4 film has been calculated by means of the following equation [37] ;

$$n = \left(\frac{1+R}{1-R}\right) - \sqrt{\frac{4R}{(1-R)^2} - k^2} \tag{2}$$

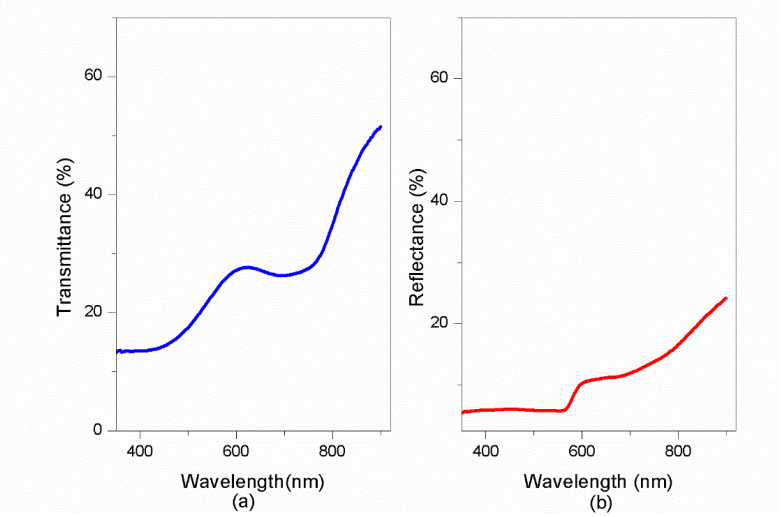

Figure 4. The transmittance spectrum (a) and reflectance spectrum (b) of the film

In this equation, k, extinction coefficient is expressed as $k = \alpha\lambda/4\pi$ equation while R is the reflectance. The refractive index and extinction coefficient values of the film are given in Figure 5 and these values changed with wavelenght. Refractive index of the film is low around wavelength of 350 nm and a gradual rise in the wavelength range of 550-800 nm. Complex dielectric constant for a material can be stated as below [38]:

$$\varepsilon^* = (n^2 - k^2) + i2nk \tag{3}$$

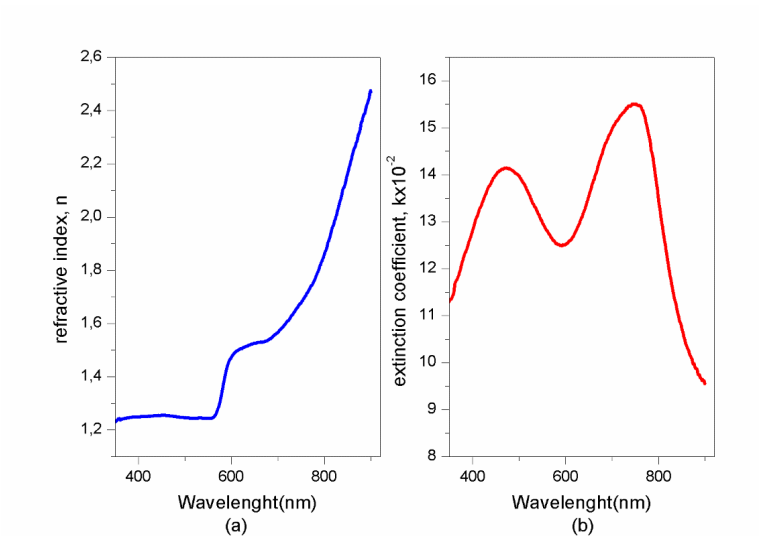

Figure 5. Variation of refractive index (a) and extinction coefficient (b) of the film with wavelength

Here, ε_1 (= n^2 - k^2) is the real part of the dielectric constant while, ε_2 (=2nk) is the imaginary part. The dependence of the ε_1 and ε_2 values on the wavelength is shown in Figure 6. The average ε_1 values are higher than those of ε_2. The imaginary part of the dielectric constant shows two peak at about 2,65 eV and 1,62 eV. Figure 7 shows the variation of the optical conductivity (σ) with wavelength. The following relation is used to calculate the optical conductivity of the film [39]:

$$\sigma = \left(\frac{\alpha n c}{4\pi} \right) \tag{4}$$

where n is the the refractive index, α is the absorption coefficient and c is the velocity of light. The optical conductivity value of the film decreased up to a minimum value of wavelength then a gradual increased, and again decreased in the visible region. The optical properties of a semiconductor film depend on the size of the nanocrystallites and film thickness.

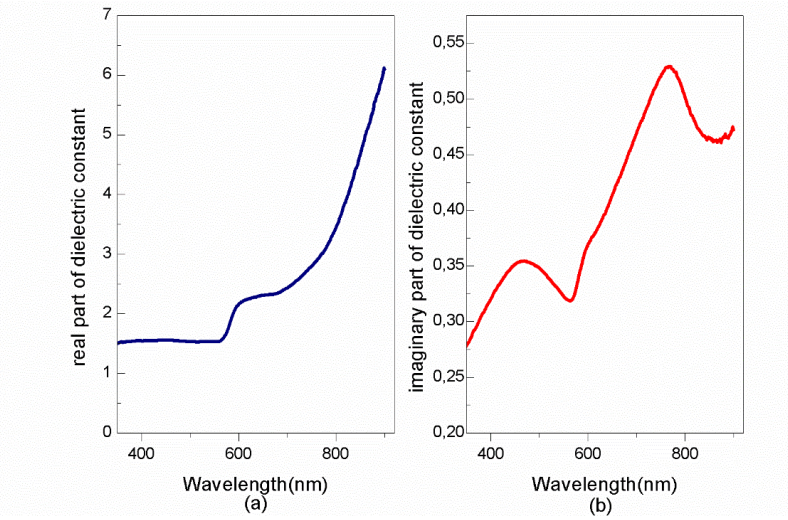

Figure 6. Variation of the real part (a) and the imaginary part (b) of the optical conductivity of the film with wavelength

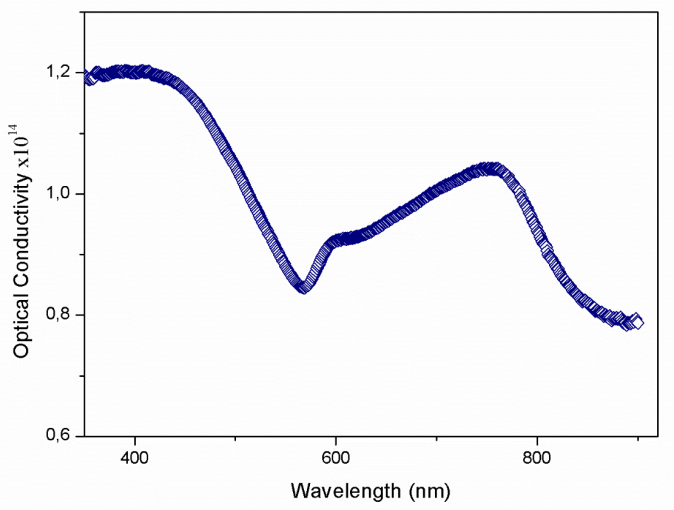

Figure 7. Optical conductivity of S-Co_3O_4 nanostructured thin film

3.4 Vibrational (Raman and FT-IR) Spectra of the Film

Raman Spectroscopy gives information on materials by means of the rotation and vibration modes of chemical bonds at infrared section. Raman scattering and IR absorption spectrums of a particle are very similar to each other. These two techniques are supplementary for each other, an IR active group can be Raman inactive while a Raman active group can be IR inactive [40]. FT-IR spectrum of the film is shown in Figure 8. The mid-FT-IR spectrum of the film is recorded in the wavenumber ranging from 500 to 3000 cm^{-1}. The characteristic vibrations at 620, 658 and 773 cm^{-1} can be assigned to Co_3O_4 [41] stretching frequencies and the band at 937 cm^{-1} to O-Si–O bond. The strong band observed at 2364 cm^{-1} corresponds to CO_2 molecule in air. In addition, Co-S stretching was not detected [19].

Raman spectrum was very spesific showing bands at 100-1000 cm^{-1} (Figure 9). It can be seen that there are five Raman peaks at 129 ($F^3{}_{2g}$), 209 ($F^3{}_{2g}$), 494 (E_g), 532 ($F^1{}_{2g}$) cm^{-1} and 699 cm^{-1} (A_{1g}), for Co_3O_4. These peaks are in agreement with the group theory [10]. There were some shifts in Raman peaks observed for Co_3O_4 due to penetration of doping atom into crystal lattice according to the peaks observed for Co_3O_4 in the literature. The minor peaks, sometime absent, around 583, 597 and 625 cm^{-1} probably relating to Co-S stretching. Particle size and interfacial bonding are important factors affecting the Raman spectrum. Raman spectroscopy results are very consistent with our XRD observations.

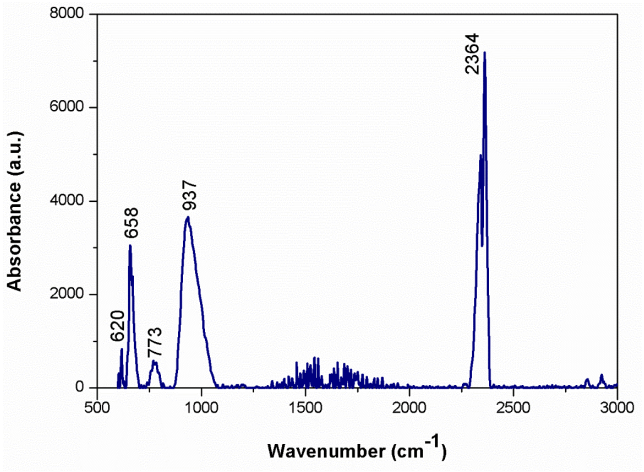

Figure 8. FT-IR spectrum of the S-Co_3O_4 nanostructured thin film

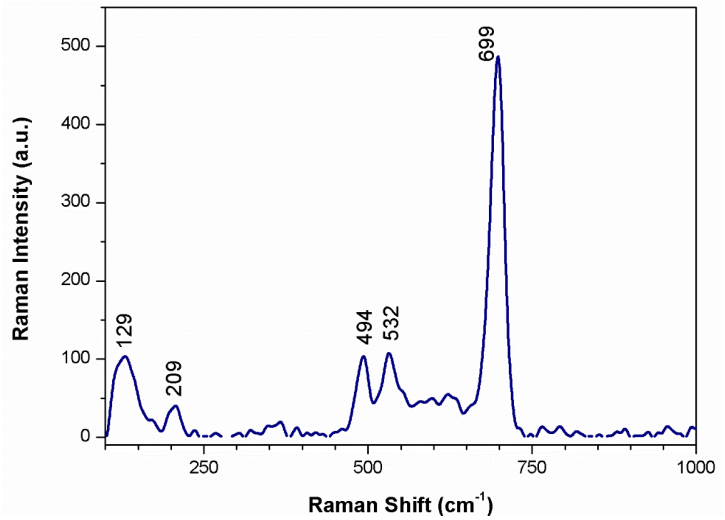

Figure 9. Raman spectrum of the S-Co_3O_4 nanostructured thin film

4. CONCLUSIONS

The film was prepared on glass substrate using USP method which draws attention by its cost efficiency and easy application. The crystallite size of the film has been determined to be 24 nm. The thicknesses of the film was approximately 215 nm. The optical constants such as refractive index, extinction coefficient, optical conductivity and dielectric constant of the film were determined using absorbance and reflectance spectra. The imaginary part of the dielectric constant shows two peak at about 2,65 eV and 1,62 eV. The characteristic vibrations at 620, 658 and 773 cm^{-1} can be assigned to Co_3O_4 stretching frequencies. In Raman spectrum five Raman peaks at 129 (F^3_{2g}), 209 (F^3_{2g}), 494 (E_g), 532 (F^1_{2g}) cm^{-1} and 699 cm^{-1} (A_{1g}) were identified respectively, for Co_3O_4. FTIR spectrum of the film has been investigated in 500–3000 cm^{-1} region and the characteristic vibrations at 620, 658 and 773 cm^{-1} can be assigned to Co_3O_4 stretching frequencies.

ACKNOWLEDGEMENTS

We would like to thank Özge Bağlayan for the vibrational, Seval Aksoy for the optical measurements.

REFERENCES

[1] Xia Y N, Yang P D, Sun Y G, Wu Y Y, Mayers B, Gates B, Yin Y, Kim F, Yan H. One-dimensional nanostructures: synthesis, characterization, and applications, Adv Mater 2003; 15: 353-389.

[2] Gürmen S, Stopic S, Friedrich B. Synthesis of nanosized spherical cobalt powder by ultrasonic spray pyrolysis, Mater Res Bulletin 2006; 41: 1882-1890.

[3] Noguero C. Physics and chemistry at oxide surfaces, Acta Crystallographica Section A 1997; 6: 855-856.

[4] Kung H H. Transition Metal Oxides: Surface Chemistry and Catalysis, Amsterdam, Netherlands: Elsevier Science, 1989.

[5] Henrich V E, Cox P A. The Surface Science of Metal Oxides, Cambridge, U.K: Cambridge University Press, 1994.

[6] Fernandez-Garcia M, Martinez-Arias A, Hanson J C, Rodriguez J A. Nanostructured oxides in chemistry: Characterization and properties, Chem Rev 2004; 104: 4063-4104.

[7] Shinde V R, Mahadik S B, Gujar T P, Lokhande C D. Supercapacitive cobalt oxide (Co_3O_4) thin films by spray pylrolysis, App Surf Sci 2006; 252: 7487-7492.

[8] Jimenez V M, Fernandez A, Espinos J P, Gonzalez-Elipe A R. The state of the oxygen at the surface of polycrystalline cobalt oxide, J Elec Spe Related Phenomena 1995; 71: 61-71.

[9] Tanaka M, Mukai M , Fujimori Y, Kondoh M, Tasaka Y, Baba H, Usami S. Transition metal oxide films prepared by pulsed laser deposition for atomic beam detection, Thin Solid Films 1996; 281-282: 453-456.

[10] Louardi A, Rmili A, Ouachtari F, Bouaoud A, Elidrissi B, Erguig H. Characterization of cobalt oxide thin films prepared by a facile spray pyrolysis technique using perfume atomizer, J Alloys Compd 2011; 509: 9183-9189.

[11] Saputra E , Muhammad S, Sun H, Ang H M, Tade M O, Wang S A. Comparative Study of Spinel Structured Mn_3O_4, Co_3O_4 and Fe_3O_4 Nanoparticles in Catalytic Oxidation of Phenolic Contaminants in Aqueous Solutions, J Colloid Interface Sci 2013; 407: 467-473.

[12] Tomic-Tucakovic B, Majstorovic D, Jelic D, Mentus S. Thermogravimetric study of the kinetics of Co_3O_4 reduction by hydrogen, Thermochimica Acta 2012; 541: 15-24.

[13] Yua Z, Dub J, Guoc S, Zhanga J, Matsumoto Y. CoS thin films prepared with modified chemical bath deposition, Thin Solid Films 2002; 415: 173-176.

[14] Li Y, Huang K, Yao Z, Liu S, Qing X. Co_3O_4 thin film prepared by a chemical bath deposition for electrochemical capacitors, Electrochimica Acta 2011; 56: 2140-2144.

[15] Kung C W, Lin C Y, Li T J, Vittal R, Ho K C. Synthesis of Co_3O_4 thin films by chemical bath deposition in the presence of different anions and application to H_2O_2 sensing, Procedia Engineering 2011; 25: 847-850.

[16] Mane S T, Kamble S S, Deshmukh L P. Cobalt sulphide thin films: Chemical bath deposition, growth and properties, Mater Lett 2011; 65: 2639-2641.

[17] Cheng C S, Serizawa M, Sakata H, Hirayama T. Electrical conductivity of Co_3O_4 films prepared by chemical vapour deposition, Mater Chem Phys 1998; 53: 225-230.

[18] Shalini K, Mane A U, Shivashankar S A, Rajeswari M, Choopun S. Epitaxial growth of Co_3O_4 films by low temperature low pressure chemical vapour deposition, J of Cry Growth 2001; 231: 242-247.

[19] Jana S, Kumar Bhar S, Mukherjee N, Mondal A. Electrodeposition of polymer encapsulated cobalt sulfide thin films: search for a frequency switching material, Mater Lett, 2013; 109: 51-54.

[20] Chae S Y, Hwang Y J, Choi J H, Joo O S. Cobalt sulfide thin films for counter electrodes of dye-sensitized solar cells with cobalt complex based electrolyte, Electrochimica Acta 2013; 114: 745-749.

[21] Shelke P N, Khollam Y B, Hawaldar R R, Gunjal S D, Udawant R R, Sarode M T, Takwale M G, Mohite K C. Synthesis, characterization and optical properties of selective Co_3O_4 films 1-D interlinked nanowires prepared by spray pyrolysis technique, Fuel 2013; 112: 542-549.

[22] Mariammal R N, Ramachandran K, Kalaiselvan G, Arumugam S, Renganathan B, Sastikumar D. Effect of magnetism on the ethanol sensitivity of undoped and Mn-doped CuO nanoflakes, Appl Surf Sci 2013; 270: 545-552.

[23] Stella C, Soundararajan N, Ramachandran K. Structural, optical, and magnetic properties of Mn and Fe-doped Co_3O_4 nanoparticles AIP Advances 2015; 5: 087104-087113.

[24] Kerli S. Boron-doped cobalt oxide thin films and its electrochemical properties, Modern Physics Letters B 2016; 30: 1650343-1650351.

[25] Chtouki T, Louardi A, Elidrissi B, Erguig H. Structural, morphological and optical properties of $Zn_xCo_{3-x}O_4$ ($0 \leq x \leq 1$) thin films prepared by spray pyrolysis technique, J of Mat Sci and Engineering A 2013; 11: 743-750.

[26] Ozer T, Köse S. Some physical properties of $Cd_{1-x}Sn_xS$ films used as window layer in heterojunction solar cells, Inter J Hyd Energy 2009; 34: 5186-5190.

[27] Birajdar S D , Khirade P P, V R Bhagwat V R, Humbe A V, Jadhav K M. Synthesis, structural, morphological, optical and magnetic properties of $Zn_{1-x}Co_xO$ (0<=x<= 0.36) nanoparticles synthesized by sol-gel auto combustion method, J Alloys and Compd 2016; 68: 513-526.

[28] Nakrela A, Benramdane N, Bouzidi A, Kebbab Z, Medles M, Mathieu C. Site location of Al-dopant in ZnO lattice by exploiting the structural and optical characterisation of ZnO:Al thin films, Results in Physics 2016; 6: 133-138

[29] Cullity B D, Stock S R. Elements of X-ray Diffraction. 2nd ed. New Jersey, USA: Prentice-Hall, 2001.

[30] Zhao G, Xu Z, Zhang L, Sun K. Hierarchical porous Co_3O_4 films with size-adjustable pores as Li ionbattery anodes with excellent rate performances, Electrochimica Acta 2013; 114: 251-258.

[31] Wua J B, Lina Y, Xiab X H, Xua J Y, Shia Q Y. Pseudocapacitive properties of electrodeposited porous nanowall Co_3O_4 film, Electrochimica Acta 2011; 56: 7163-7170.

[32] Unuma H, Saito Y, Watanabe K, Sugawara M. Preparation of Co_3O_4 thin films by a modified chemical-bath method, Thin Solid Films 2004; 468: 4-7.

[33] Wang S, Zhang B, Zhao C, Li S, Zhang M, Yan L. Valence control of cobalt oxide thin films by annealing atmosphere, App Surf Sci 2011; 257: 3358-3362.

[34] Kadam L D, Patil P S. Thickness-dependent properties of sprayed cobalt oxide thin films, Mater Chem and Phys 2001; 68: 225-232.

[35] Kerli S. Boron-doped cobalt oxide thin films and its electrochemical properties, Modern Physics Letters B. 27 2016; 30: 1650343-1650350.

[36] Stella C, Soundararajan N, Ramachandran K, Structural, optical, and magnetic properties of Mn and Fe-doped Co_3O_4 nanoparticles, AIP Advances 2015; 5: 087104-087113.

[37] Caglar M, Caglar Y, Ilican S. Investigation of the effect of Mg doping for improvements of optical and electrical properties, Physica B 2016; 485: 6-13.

[38] Yakuphanoglu F, Ilican S, Caglar M, Caglar Y. Microstructure and electro-optical properties of sol–gel derived Cd-doped ZnO films, Superlattices and Microstructures 2010; 47: 732-743.

[39] Girisun T C S, Dhanuskodi S. Linear and Nonlinear Optical Properties of Tristhiourea Zinc Sulphate (ZTS) Single, Cry Resear Tech, 2009; 44: 1297-1302.

[40] Gündüz T. İnstrumental Analiz. 9nd ed. Ankara, Turkey: Fersa Press, 2005.

[41] Yuan Y F, Xia X H, Wu J B, Gud J S, Chen Y B, Guo SY. Electrochromism in mesoporous nanowall cobalt oxide thin films prepared via lyotropic liquid crystal media with electrodeposition, J of Membrane Sci 2010; 364: 298-303.